HOKKAIDO UNIVERSITY

Title	Double nuclear spin switching in single quantum dots
Author(s)	Yamamoto, S.; Kaji, R.; Sasakura, H. et al.
Citation	Japanese Journal of Applied Physics, 60(SB), SBBH07 https://doi.org/10.35848/1347-4065/abd709
Issue Date	2021-01-15
Doc URL	https://hdl.handle.net/2115/84424
Rights	© 2021 The Japan Society of Applied Physics
Rights(URL)	https://creativecommons.org/licenses/by-nc-nd/4.0/
Type	journal article
File Information	SY_JJAP60SBBH07.pdf

Hokkaido University Collection of Scholarly and Academic Papers : HUSCAP

Double nuclear spin switching in single quantum dots

S. Yamamoto[1,*], R. Kaji[1], H. Sasakura[1], and S. Adachi[1]

[1] *Division of Applied Physics, Graduate School of Engineering, Hokkaido University, N13 W8, Kitaku, Sapporo 060-8628, Japan*
E-mail: yama-st@eis.hokudai.ac.jp

Hyperfine interaction in a quantum dot produces a spin-coupled system between an injected electron and a few tens of thousands of nuclei in the electron wavefunction. We report here that the double bistable phenomenon of nuclear spin polarization (NSP) can be observed by sweeping three control parameters. All the observations indicate that the NSP has three stable branches under a longitudinal magnetic field, whereas the number of the stable branches of NSP has been believed to be two at most. The incorporation of the electron spin relaxation due to the nuclear spin fluctuation enables reproduction of the observed features of the NSP and the electron spin polarization.

1. Introduction

Electron–nuclear spin coupling by hyperfine interaction (HFI) is highly important in quantum dots (QDs). This is because the spin flip–flop process via HFI transfers the spin angular momentum from a confined electron to the lattice nuclear spin ensemble.[1,2] Consequently, nuclear spin polarization (NSP) can be induced easily by optical spin-selective electron injection.[3–5] The NSP affects the electron spin states as an effective magnetic field (i.e., a nuclear field) and enables various applications, such as quantum memory, owing to the unprecedented long-duration spin coherence.[6–8] Recent demonstration and prediction suggest the possibility of a quantum read–write process with over 90% accuracy.[9,10]

One of the most interesting properties of NSP is bistability, known as nuclear spin switching (NSSW), in which the NSP transits abruptly between two concurrently present stable branches owing to the negative and positive feedbacks of the spin transfer rate.[11–16] NSSW occurs when the electronic Zeeman splitting, which limits the spin transfer rate, is reduced owing to the compensation of the external magnetic field by a nuclear field.

The nuclear field, $\boldsymbol{B}_{\rm n}$, consists of a static part $\boldsymbol{B}_{\rm n}^{\rm stat}$ and a fluctuating part $\boldsymbol{B}_{\rm f}$. The nuclear spin fluctuation is known to cause severe electron spin decoherence,[17,18] which is an undesired aspect of HFI. Although it is essential to determine completely the formation and relaxation processes of NSP for controlling NSP and electron spin polarization, the nuclear spin fluctuation has not been related to the NSP formation dynamics yet.[16]

In this study, we show that the effect of the nuclear spin fluctuation on an electron, in turn, affects the NSP dynamics and generates an extra stable branch. This suggests that the NSP in the individual QDs potentially has three stable branches. This unique behavior is demonstrated by steady-state photoluminescence (PL) measurements. In previous studies,[19,20] we focused on the excitation power dependence of NSP. Extending from the study in Ref.,[19] the dependencies on the excitation polarization, external magnetic field, as well as excitation power are discussed in detail. In addition, the proposed model predicts that a QD spin system exhibits a *tristable* response under some conditions.

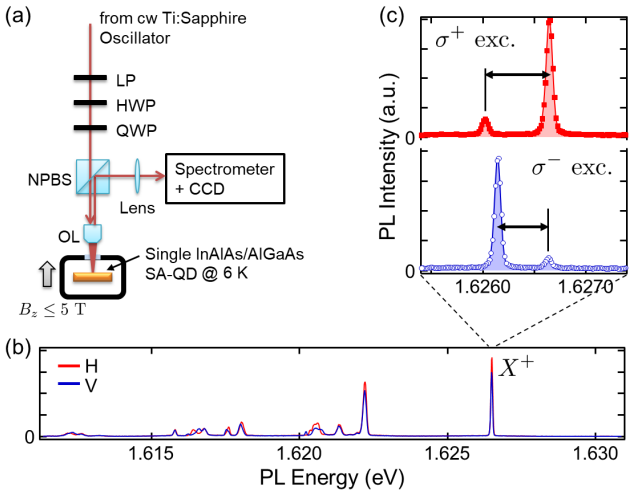


Fig. 1. (color online) (a) Experimental setup for μ-PL measurements under a longitudinal magnetic field. (b) PL spectra from a single QD detected in linearly polarized basis under unpolarized excitation at 0 T. (c) Zeeman-split PL spectra of X^+ under σ^+ (upper panel) and σ^- (lower panel) excitations at B_z = +4 T with $P_{\rm exc}$=350 μW. PL peak in higher (lower) energy side is $\sigma^{+(-)}$-polarized. Zeeman splitting energy indicated by arrow differs depending on excitation helicity.

2. Sample and Experimental Apparatus

Molecular-beam epitaxy-grown $In_{0.75}Al_{0.25}As/Al_{0.3}Ga_{0.7}As$ self-assembled (SA) QDs on (100) GaAs substrate were used in the experiments. The InAlAs QDs have lens-like shapes with the typical diameter of 20 nm and a height of 4 nm.[4,21] The fabrication of small mesa structures allows characterizing single QDs by micro-PL measurements. A continuous wave Ti:sapphire laser was used to inject optically a spin-polarized electron and hole into the wetting layer of the QDs (~1.6986 eV). The excitation polarization was controlled precisely by combining a linear polarizer (LP), half-waveplate (HWP), and quarter-waveplate (QWP), as shown in Fig. 1(a). The HWP was used to cancel out the undesired phase distortion caused by the optical elements, such as mirrors and beam splitter (BS) in the excitation beam path. The excitation beam was focused on the QD sample along the growth direction (z) by an objective lens (OL, ×20). The sample was kept at 6 K in an optical cryostat, which was inserted in a superconducting magnet introducing a static longitudinal magnetic field B_z up

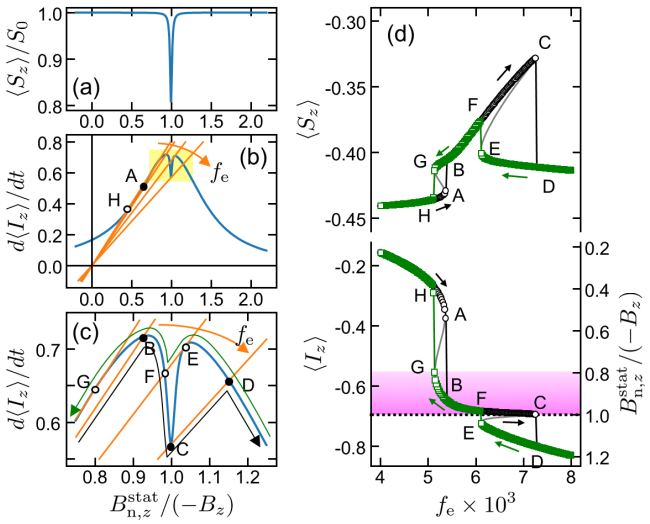


Fig. 2. (color online) (a) Calculated $\langle S_z\rangle$ normalized by S_0. (b), (c) Schematics of NSP formation (blue curve) and relaxation terms (orange lines). (c) is closeup view of square region in (b). Steady-state solutions are interpreted as intersections of two terms, and inclination of relaxation term depends on f_e, which is indicated by arrows. Solid (open) circles represent intersections with increasing (decreasing) f_e, and arrowed black (green) trace indicates the state-tracking route. (d) f_e dependencies of $\langle S_z\rangle$ (top) and $\langle I_z\rangle$ (bottom) under σ^+ excitation. Labeled points correspond to those in (b) and (c). In lower panel, solutions in shaded region represent new stable branch.

to 5 T. The PL from the individual QDs collected by the same objective lens was dispersed by a triple grating spectrometer and detected by a liquid-nitrogen cooled CCD. Although the energy resolution of our apparatus was ~12 μeV, the peak energy could be determined with an accuracy of less than 5 μeV using spectral fittings.

Figure 1(b) shows the typical PL spectra from a single QD. The most intense PL peak is attributed to the positive trion, X^+, consisting of one electron and spin-singlet two holes. We focus on the X^+ PL. This is because the z component of the electron spin polarization, $\langle S_z\rangle$, is related to the degree of circular polarization, ρ_c, through $\langle S_z\rangle = \rho_c/2$ when $\rho_c \equiv (I^- - I^+)/(I^- + I^+)$, where $I^{-(+)}$ is the $\sigma^{-(+)}$ PL intensity.

Figure 1(c) shows the X^+ PL spectra at $B_z = +4$ T. It is seen clearly, the Zeeman splitting under the σ^+ excitation is larger than that under the σ^- excitation. This can be explained by the Overhauser shift, Δ_{OS}, due to an optically generated $B^{stat}_{n,z}$ whose direction is dependent on the excitation polarization (i.e., the orientation of the spin of the photo-injected electron).[3–5,16)]

3. Theoretical Explanation of Double NSSW

The formation dynamics of NSP can be expressed by the phenomenological rate equation,[16,22)]

$$\frac{d\langle I_z\rangle}{dt} = \frac{1}{T_{NF}}[Q(\langle S_z\rangle - \langle S_z^{eq}\rangle) - \langle I_z\rangle] - \frac{1}{T_{ND}}\langle I_z\rangle. \quad (1)$$

Above, Q is a material-dependent constant, which is ~16 for our InAlAs. $1/T_{NF}$ and $1/T_{ND}$ are the formation and decay rates of the NSP, respectively. The thermal equilibrium value, $\langle S_z^{eq}\rangle$, of $\langle S_z\rangle$ is neglected hereafter. The formation rate, $1/T_{NF}$, given by

$$\frac{1}{T_{NF}} = \frac{2f_e\tau_c(A/N)^2}{\hbar^2 + [g_e\mu_B(B_z + B^{stat}_{n,z})\tau_c]^2} \quad (2)$$

suggests that the spin transfer is maximized when the electron spin splitting, $g_e\mu_B(B_z+B^{stat}_{n,z})$, becomes zero. Such a scenario can be achieved if $B^{stat}_{n,z}=2A\langle I_z\rangle/(g_e\mu_B)$ cancels out B_z. Here, f_e is the time fraction when an unpaired electron spin occupies the QD, τ_c is the correlation time between the electron and nuclear spins, $A \sim 50$ μeV is the hyperfine constant, N is the number of nuclei in the localization volume, g_e is the g-factor of a conduction electron, and $\hbar$ and μ_B are the reduced Planck constant and the Bohr magneton, respectively.

Most of the previous studies treated $\langle S_z\rangle$ in Eq. (1) as a constant and explained two coexistent stable branches.[4,5,11–16)] However, as has been revealed previously, $\langle S_z\rangle$ can be reduced owing to the effect of the nuclear spin fluctuation.[17,18)] Although the temporal change in the fluctuating field is much slower than the annihilation of a single electron spin, the ensemble average, $\langle S_z\rangle$, over numerous electron generation–annihilation cycles in the exposure time of the detector decreases owing to the fluctuation of the nuclear field. Because the expected magnitude of $\boldsymbol{B}_f$ is the order of 10–100 mT,[24–28)] the reduction in $\langle S_z\rangle$ should be limited near the condition, $B_z+B^{stat}_{n,z} = 0$.

We treat this effect by separating the nuclear field into a stationary part $\boldsymbol{B}^{stat}_n$ and a fluctuating part $\boldsymbol{B}_f$.[23)] From the steady-state solution of the Bloch equation, we assume

$$\langle S_z\rangle = S_0\frac{B^2_{1/2} + \langle B^2_{f,z}\rangle + (B_z + B^{stat}_{n,z})^2}{B^2_{1/2} + \langle B^2_f\rangle + (B_z + B^{stat}_{n,z})^2}. \quad (3)$$

Here, S_0 is the upper limit of the electron spin polarization determined by the injected polarization, S_i, and the electron spin coherence time. $B_{1/2} = \hbar/(g_e\mu_B\tau_e)$ is a reduced field of the electron spin lifetime, τ_e. $\langle B^2_f\rangle = 3\langle B^2_{f,z}\rangle$ is the expectation value of the square of the fluctuation amplitude where the isotropic spatial distribution of $\boldsymbol{B}_f$ is assumed. As shown in Fig. 2(a), $\langle S_z\rangle$ expressed by Eq. (3) presents a steep decay around the point, $B^{stat}_{n,z}/(-B_z) = 1$.

Figures 2(b) and 2(c) show the schematics of the normalized formation term (blue curve) and the relaxation term (orange straight lines) of Eq. (1). The wide Lorentzian shape of the formation term reflects $1/T_{NF}$, and only by this structure, a single NSSW with two stable and one unstable branches can be explained, as has been discussed previously.[16)] A narrow dip in the formation term, which is the key point of this study, originates from the $\langle S_z\rangle$ reduction due to the nuclear spin fluctuation. Concurrently, the relaxation term is represented by a straight line whose inclination changes in response to the change in f_e because of the normalization of the formation term in the figures. The increase in f_e corresponds to the large tilting of the relaxation term, as shown by arrows in Figs. 2(b) and 2(c). The steady-state NSP observed in the time-integrated PLs is interpreted as intersections of the formation and relaxation terms.

Let us consider the trajectory of an intersection with f_e, which is controlled by the excitation power, P_{exc}. Starting from the lower f_e where the system takes a unique solution, the intersection follows the formation curve with increasing f_e until point A, following which it jumps to point B. Sub-

sequently, the state moves to point C along the dip structure and finally jumps to point D, as shown by the black trace. However, returning from the larger f_e, the system maintains a continuous state of evolution until point E, and the state-tracking route of E→F→G→H (green trace) is obtained. The trajectories of these intersections and the accompanying $\langle S_z \rangle$ are plotted as a function of f_e in Fig. 2(d).

From these considerations, we found that the plateau of the NSP between points B and C originates from the narrow dip centered at $B^{stat}_{n,z}/(-B_z) = 1$. Because a large decay in $\langle S_z \rangle$ occurs at this point, as shown in the top panel of Fig. 2(d), it is difficult for the NSP to increase and overcome the cancellation point, even on increasing f_e. Thus, the saturation of $\langle I_z \rangle$ occurs, leading to the appearance of the extra stable branch. The above-mentioned features of the NSP are considered to be common for various QD systems because the developed model is not associated with specific materials or lattice structures. The details of the model calculations and the derivation of the equations are described in Ref. 20.

4. Observations of Double NSSW

Figure 3(a) shows the excitation power, P_{exc}, dependencies of ρ_c (= $2\langle S_z \rangle$) and Δ_{OS}. While Δ_{OS} under σ^- excitation increases monotonically with increasing P_{exc}, $|\Delta_{OS}|$ under σ^+ excitation exhibits clear jumps accompanying the abrupt drops of $|\rho_c|$. Clearly, the NSSW occurs twice, which suggests three stable branches although only one NSSW and two stable branches are believed.[11–16] Double switching labels, I and II, can be regarded as hysteresis loops ABGH and CDEF in Fig. 2(d), respectively. Also, the branch named Mid. in Fig. 3(a) corresponds to the plateau of the NSP between points B and C in Fig. 2(d).

Figure 3(b) shows the change in $|\rho_c|$ depending on the electronic Zeeman splitting, $\Delta_{Zeeman} \equiv g_e\mu_B B_z + \Delta_{OS} = g_e\mu_B(B_z + B^{stat}_{n,z})$. The data were obtained from P_{exc} dependencies at different magnetic fields as indicated in the figure. Circles, squares, and triangles represent the Lo., Mid., and Hi.-branches, respectively. As clearly shown, $|\rho_c|$ decreases sharply as $|\Delta_{Zeeman}|$ approaches zero, where the complete compensation of B_z by $B^{stat}_{n,z}$ is fulfilled. This sharp reduction is a clear indication of the effect of the nuclear spin fluctuation, which is treated by Eq. (3) and expected to cause a steep decay of $\langle S_z \rangle$, as shown in Fig. 2(a). The data in Mid.-branch are in the vicinity of Δ_{Zeeman}=0 and highlight the entire decay curve of $|\rho_c|$, which is very different from our previous measurements.[24,25]

It is worth noting that the double NSSW is not always observed. Figure 3(c) shows a single switching of Δ_{OS}, which is observed in the same QD as Fig. 3(a) under σ^+ excitation but at B_z=+2.5 T. Under a low magnetic field, all of the measured QDs indicated single switching similar to Fig. 3(c), and the threshold B_z from single to double switching was dependent on the parameters of the individual QDs. Furthermore, the majority of the QDs showed only single NSSW under our available B_z of 5 T.

The double NSSW was also observed on changing the excitation polarization and the magnetic field. Figure 3(d) shows the excitation polarization dependencies of ρ_c (upper panel) and Δ_{OS} (lower panel) at B_z = +3.5 T. Here, the excitation polarization, ρ_c^{exc}, is defined as the same definition of ρ_c, and thus ρ_c^{exc} = ∓1 corresponds to the $\sigma^{\pm}$ excitation. Although

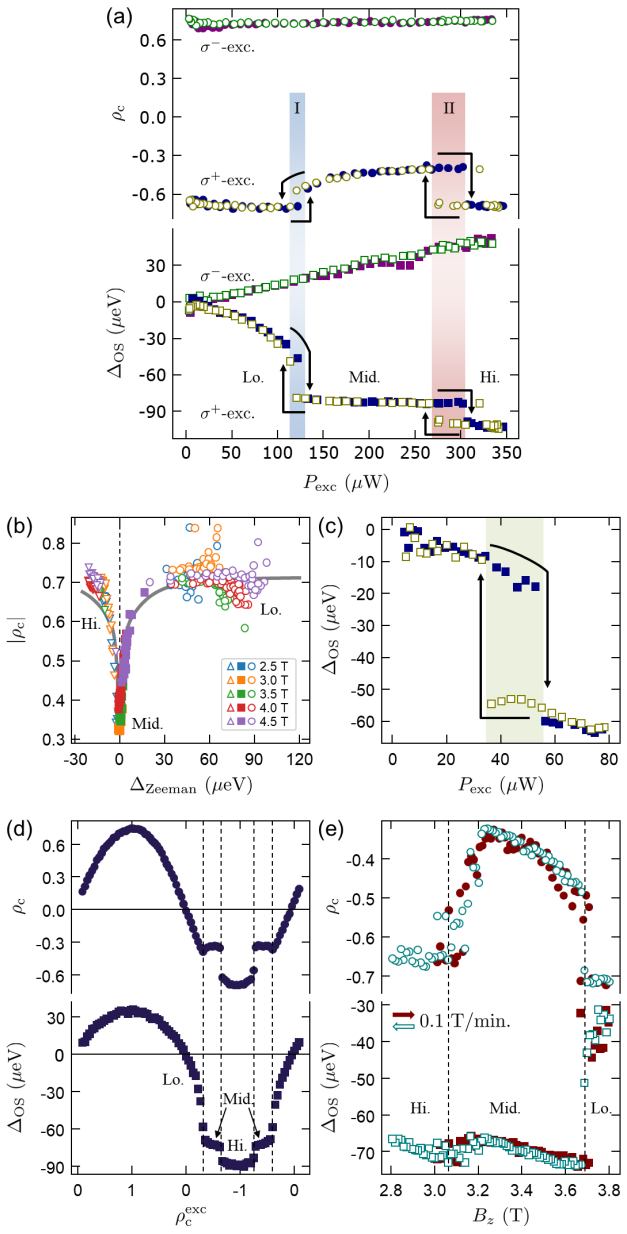


Fig. 3. (color online) (a) P_{exc} dependencies of ρ_c (upper panel) and Δ_{OS} (lower panel) at B_z = +4.0 T. (b) $|\rho_c|$ plotted as function of electronic Zeeman splitting Δ_{Zeeman}. (c) P_{exc} dependence of Δ_{OS} at B_z = +2.5 T under σ^+ excitation. (d) Excitation polarization dependencies of ρ_c (upper panel) and Δ_{OS} (lower panel) at B_z = +3.5 T. Horizontal axis ρ_c^{exc} is the circular polarization degree of excitation light where ρ_c^{exc} = ∓1 corresponds to $\sigma^{\pm}$ excitation. (e) B_z dependence of ρ_c (upper panel) and Δ_{OS} (lower panel). Sweeping rate of B_z is 0.1 T/min.

the σ^- excitation did not exhibit any switching because the generated $B^{stat}_{n,z}$ pointed to the same direction as B_z, and clear switching was observed around the σ^+ excitation where $B^{stat}_{n,z}$ and B_z pointed to opposite directions. Figure 3(e) shows ρ_c (upper panel) and Δ_{OS} (lower panel) that were observed with increasing and decreasing B_z, respectively. The σ^+ excitation and a sweeping rate of B_z (0.1 T/min), which is sufficiently slow for the NSP to follow its steady-state branch, were employed. The figure shows that the NSP requires the Hi.-branch in the low B_z region and transits to the Lo.-branch through the Mid.-branch as B_z increases. With decreasing B_z, the NSP retraces these three branches in the reverse order.

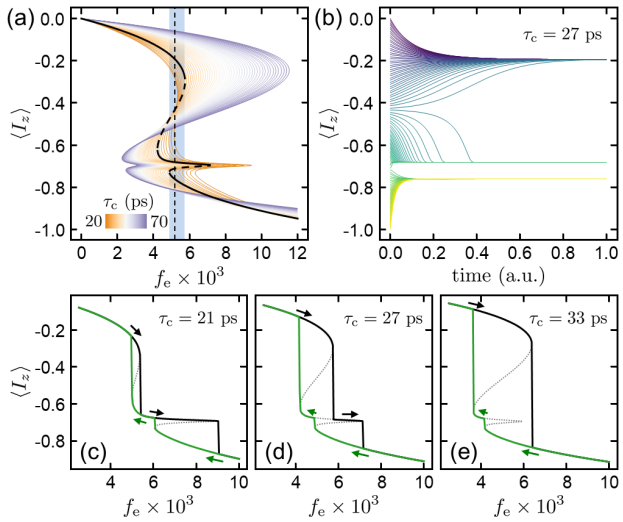


Fig. 4. (color online) (a) Calculated $\langle I_z \rangle$ with various τ_c (20–70 ps). Thick black curve is example of solution with tristability, which adopts three steady-state solutions in shaded region around vertical dashed line. (b) Temporal evolution of $\langle I_z \rangle$ from different initial states with τ_c=27 ps. (c)–(e) Transition from double to single switching by controlling τ_c. Black and green curves represent the stable NSP states with increasing and decreasing f_e as shown by arrows.

From these experimental observations, it seems that the discrimination between the Mid. and Hi.-branch was rather difficult to detect in Δ_{OS} because of the small difference. However, ρ_c can probe the existence of the Mid.-branch with excellent clarity. For the Mid-branch, the nuclear spin fluctuation effectively reduces ρ_c because $B^{stat}_{n,z}+B_z \sim 0$ is achieved.

5. Toward Tristability

Finally, we present the tristability of the NSP, which is predicted from the proposed model. Figure 4(a) shows the steady-state solution of $\langle I_z \rangle$ calculated with various τ_c in the excitation power dependence. As indicated, the total shape of $\langle I_z \rangle$ strongly depends on τ_c, and the presence of the Mid.-branch fades off as τ_c increases. In the figure, the thick curve, where τ_c=27 ps is assumed, shows an example of the tristability. In the shaded region, $\langle I_z \rangle$ takes three stable and two unstable solutions. Figure. 4(b) shows the temporal evolution of $\langle I_z \rangle$ from the different initial states. As clearly shown, almost all the states converge to three stable solutions, and thus, two unstable solutions are barely observed.

The calculated results in Figs. 4(c)–4(e) demonstrate the transition from the double to the single NSSW by changing τ_c. From the comparison with Fig. 3(a), it is considered that the experimentally observed behavior of the NSP corresponds to the case of short τ_c. By increasing τ_c from this short τ_c case shown in Fig. 4(c), the state-tracking route on the Mid.-branch splits when $\langle I_z \rangle$ obtains the tristability, as shown in Fig. 4(d). Further increment in τ_c hides the Mid.-branch in the hysteresis loop, and eventually the switching behavior converges to the well-known single NSSW (bistability), as shown in Fig. 4(e). As demonstrated in the previous experiments, τ_c can be controlled by the sample temperature[29] and/or the bias voltage of charge tunable QDs.[30] These methods for the control of τ_c may reveal the transition of switching characters.

6. Conclusion

In single InAlAs SAQDs, we found that the NSP takes three stable branches although the number of branches has been believed to be two at the maximum. This was observed as a double NSSW by changing the excitation polarization and the magnitude of the applied longitudinal magnetic field as well as the excitation power. The observations were successfully explained by the phenomenological model based on the dynamic formation of the NSP, including the effect of the nuclear spin fluctuation. The double NSSW is considered to be general in various QD systems because the developed model is not related to specific materials or lattice structures. Furthermore, the model predicts tristability of the NSP whose high degree of freedom may open routes for more elaborate spin operations in the QD system.

This work was supported by JSPS KAKENHI (Grants No. JP26800162 and No.JP17K19046)

1) *Spin Physics in Semiconductors*, Springer Series in Solid-State Sciences Vol. 157, Chaps. 1 and 12, edited by M. I. Dyakonov (Springer, Berlin, 2nd ed., 2017).
2) *Optical Orientation*, Modern Problems in Condensed Matter Sciences Vol. 8, Chaps. 2 and 5, edited by F. Meier and B. Zakharchenya (North-Holland, NewYork, 1984).
3) D. Gammon, Al. L. Efros, T. A. Kennedy, M. Rosen, D. S. Katzer, D. Park, S. W. Brown, V. L. Korenev, and I. A. Merkulov, Phys. Rev. Lett. **86**, 5176 (2001).
4) T. Yokoi, S. Adachi, H. Sasakura, S. Muto, H. Z. Song, T. Usuki, and S. Hirose, Phys. Rev. B **71**, 041307(R) (2005).
5) B. Eble, O. Krebs, A. Lemaître, K. Kowalik, A. Kudelski, P. Voisin, B. Urbaszek, X. Marie, and T. Amand, Phys. Rev. B **74**, 081306(R) (2006).
6) *Semiconductor Spintronics and Quantum Computation*, edited by D. D. Awschalom, D. Loss, and N. Samarth (Springer-Verlag, Berlin, 2002).
7) J. M. Taylor, C. M. Marcus, and M. D. Lukin, Phys. Rev. Lett. **90**, 206803 (2003).
8) C. Boehme and D. R. McCamey, Science **336**, 1239 (2012).
9) D. A. Gangloff, G. Éthier-Majcher, C. Lang, E. V. Denning, J. H. Bodey, D. M. Jackson, E. Clarke, M. Hugues, C. Le Gall, and M. Atatüre, Science **364**, 62 (2019).
10) E. V. Denning, D. A. Gangloff, M. Atatüre, J. Mørk, and C. Le Gall, Phys. Rev. Lett. **123**, 140502 (2019).
11) P.-F. Braun, B. Urbaszek, T. Amand, X. Marie, O. Krebs, B. Eble, A. Lemaître, and P. Voisin, Phys. Rev. B **74**, 245306 (2006).
12) A. I. Tartakovskii, T. Wright, A. Russell, A. B. Van'kov, J. Skiba-Szymanska, I. Drouzas, R. S. Kolodka, M. S. Skolnick, P. W. Fry, A. Tahraoui, H.-Y. Liu, and M. Hopkinson, Phys. Rev. Lett. **98**, 026806 (2007).
13) P. Maletinsky, C. W. Lai, A. Badolato, and A. Imamoglu, Phys. Rev. B **75**, 035409 (2007).
14) R. Kaji, S. Adachi, H. Sasakura, and S. Muto, Phys. Rev. B **77**, 115345 (2008).
15) T. Belhadj, T. Kuroda, C.-M. Simon, T. Amand, T. Mano, K. Sakoda, N. Koguchi, X. Marie, and B. Urbaszek, Phys. Rev. B **78**, 205325 (2008).
16) B. Urbaszek, X. Marie, T. Amand, O. Krebs, P. Voisin, P. Maletinsky, A. Högele, A. Imamoglu, Rev. Mod. Phys. **85**, 79 (2013).
17) I. A. Merkulov, Al. L. Efros, and M. Rosen, Phys. Rev. B **65**, 205309 (2002).
18) A. Bechtold, D. Ranuch, F. Li, T. Simmet, P.-L. Ardelt, A. Regler, K. Muller, N. A. Sinitsyn, and J. J. Finley, Nat. Phys. **11**, 1005 (2015).
19) S. Yamamoto, R. Kaji, H. Sasakura, and S. Adachi, Ext. Abstr. Solid State Devices and Materials, 2020, p. 527.
20) S. Yamamoto, R. Kaji, H. Sasakura, and S. Adachi, Phys. Rev. B **101**, 245424 (2020).
21) H. Sasakura, S. Adachi, S. Muto, H. Z. Song, T. Miyazawa, and

Y. Nakata, Physica E (Amsterdam) **21**, 511 (2004).
22) A. Abragam, *Principles of Nuclear Magnetism* (Oxford University Press, Oxford, 1961), Chap. 8.
23) M. S. Kuznetsova, K. Flisinski, I. Ya. Gerlovin, I. V. Ignatiev, K. V. Kavokin, S. Yu. Verbin, D. R. Yakovlev, D. Reuter, A. D. Wieck, and M. Bayer, Phys. Rev. B **87**, 235320 (2013).
24) R. Kaji, S. Adachi, H. Sasakura, S. Muto, Phys. Rev. B **85**, 155315 (2012).
25) R. Kaji, R. Matsusaki, S. Yamamoto, and S. Adachi, Jpn. J. Appl. Phys. **58**, SBBH05 (2019).
26) O. Krebs, B. Eble, A. Lemaître, B. Urbaszek, K. Kowalik, A. Kudelski, X. Marie, T. Amand, and P. Voisin, Phys. Stat. Solidi. A **204**, 202 (2007).
27) O. Krebs, B. Eble, A. Lemaître, P. Voisin, B. Urbaszek, T. Amand, and X. Marie, C. R. Physique **9**, 874 (2008).
28) B. Pal, S. Y. Verbin, I. V. Ignatiev, M. Ikezawa, and Y. Masumoto, Phys. Rev. B **75**, 125322 (2007).
29) B. Urbaszek, P.-F. Braun, T. Amand, O. Krebs, T. Belhadj, A. Lemaître, P. Voisin, and X. Marie, Phys. Rev. B **76**, 201301(R) (2007).
30) J. Nilsson, L. Bouet, A. J. Bennett, T. Amand, R. M. Stevenson, I. Farrer, D. A. Ritchie, S. Kunz, X. Marie, A. J. Shields, and B. Urbaszek, Phys. Rev. B **88**, 085306 (2013).